Journal of Peptide Science
J. Peptide Sci. **10**: 546–565 (2004)
Published online 2 April 2004 in Wiley InterScience (www.interscience.wiley.com). DOI: 10.1002/psc.564

JOURNAL OF PEPTIDE SCIENCE

β-Hairpin Folding and Stability: Molecular Dynamics Simulations of Designed Peptides in Aqueous Solution

CLARA M. SANTIVERI,[a,§] M. ÁNGELES JIMÉNEZ,[a] MANUEL RICO,[a] WILFRED F. VAN GUNSTEREN[b] and XAVIER DAURA[c]*

[a] Instituto de Química Física Rocasolano, Consejo Superior de Investigaciones Científicas, E-28006 Madrid, Spain
[b] Laboratory of Physical Chemistry, Swiss Federal Institute of Technology Zurich, ETH Hönggerberg, CH-8093 Zurich, Switzerland
[c] Catalan Institution for Research and Advanced Studies (ICREA) and Institute of Biotechnology and Biomedicine, Universitat Autònoma de Barcelona, E-08193 Bellaterra, Barcelona, Spain

Received 10 September 2003
Revised 17 November 2003
Accepted 1 December 2003

Abstract: The structural properties of a 10-residue and a 15-residue peptide in aqueous solution were investigated by molecular dynamics simulation. The two designed peptides, SYINSDGTWT and SESYINSDGTWTVTE, had been studied previously by NMR at 278 K and the resulting model structures were classified as 3 : 5 β-hairpins with a type I + G1 β-bulge turn. In simulations at 278 K, starting from the NMR model structure, the 3 : 5 β-hairpin conformers proved to be stable over the time period evaluated (30 ns). Starting from an extended conformation, simulations of the decapeptide at 278 K, 323 K and 353 K were also performed to study folding. Over the relatively short time scales explored (30 ns at 278 K and 323 K, 56 ns at 353 K), folding to the 3 : 5 β-hairpin could only be observed at 353 K. At this temperature, the collapse to β-hairpin-like conformations is very fast. The conformational space accessible to the peptide is entirely dominated by loop structures with different degrees of β-hairpin character. The transitions between different types of ordered loops and β-hairpins occur through two unstructured loop conformations stabilized by a single side-chain interaction between Tyr2 and Trp9, which facilitates the changes of the hydrogen-bond register. In agreement with previous experimental results, β-hairpin formation is initially driven by the bending propensity of the turn segment. Nevertheless, the fine organization of the turn region appears to be a late event in the folding process.

Keywords: peptide folding; β-hairpin; decapeptide; pentadecapeptide; molecular dynamics; GROMOS; NMR structure

INTRODUCTION

Unravelling the factors contributing to the formation and stability of β-sheet motifs in peptides is currently a field of intense activity. The great interest of this subject arises from the relations that can be established with more complex phenomena. Thus, the folding of secondary structures captures much of the basic physics of protein folding. The study of the structural properties of β-sheet-forming peptides, as well as helix-forming ones, may contribute to a better understanding of the mechanisms by which a polypeptide chain adopts its three-dimensional native structure. This knowledge is likely to smooth the way towards successful protein structure prediction from protein sequence, which is of great importance for structural genomics.

*Correspondence to: Xavier Daura, Catalan Institution for Research and Advanced Studies and Institute of Biotechnology and Biomedicine, Universitat Autònoma de Barcelona, E-08193 Bellaterra, Barcelona, Spain; e-mail: Xavier.Daura@uab.es
§ MRC Centre for Protein Engineering, Cambridge CB2 2QH, UK
Contract/grant sponsor: Schweizer Nationalfonds; Contract/grant number: 2000-063590.00.
Contract/grant sponsor: Spanish DGYCT; Contract/grant number: PB98-0677.
Contract/grant sponsor: European project CEE; Contract/grant number: B104-97-2086.

Moreover, β-sheet structures play an important role in the formation of amyloid fibrils. Accordingly, β-sheet-forming peptides may be suitable systems for studying the molecular basis of amyloid diseases such as Alzheimer's and various spongiform encephalopathies [1,2].

In contrast to α-helices, for which substantial progress in understanding the factors involved in their formation and stability has been made through the study of the conformational behaviour of protein fragments and designed peptides [3–8], little is known about the formation of β-sheet structures. This is partly a consequence of the low solubility and high tendency to aggregate of sequences with high β-sheet-propensities. Despite the difficulties of designing peptide sequences that fold in aqueous solution into monomeric β-sheet motifs, examples of these had already been reported in the 1990s [9–14]. Most of them adopt the simplest antiparallel β-sheet structure, the β-hairpin, that consists of two β-strands linked by a turn segment. β-Hairpin motifs differ in the topology of the turn segment, and are classified according to the number of turn residues and the number of interstrand hydrogen bonds between residues flanking the turn [15–17]. The study of the kinetics of β-hairpin formation has only become possible with the development of new microsecond experimental techniques [18].

Computer simulations are playing an expanding role in biochemistry due to the steady and rapid increase in computing power and the improvement of force fields over the past years. Molecular dynamics (MD) simulation has proven to be a useful tool to study peptide folding in solution under reversible conditions at atomic resolution and to test models of the folding process. MD simulation of peptide stability and folding is currently an area of intense activity, and computational studies on helix-forming peptides [19–25] and sheet-forming peptides [21,26–37] have been reported recently.

Here, a series of MD simulations of the 10-residue peptide SYINSDGTWT and the 15-residue peptide SESYINSDGTWTVTE, using the GROMOS96 package of programs and force field [38], are presented. An important feature of these systems is that the decapeptide encompasses the middle region of the amino acid sequence of the pentadecapeptide [39], allowing us to investigate by MD simulation the stabilizing effect of strand lengthening on β-hairpin structure [39,40]. This effect has been reported recently for other β-hairpin-forming peptides [41]. The structure of the two studied peptides in aqueous solution was determined by NMR [39,40]. The resulting model structure was classified in both cases as a 3 : 5 β-hairpin with a type I + G1 β-bulge turn, one of the most abundant in proteins. The percentage population of the β-hairpin was estimated from several NMR parameters to be around 45% for the decapeptide in water at pH 6.3 and 278 K and 54% for the pentadecapeptide in water at pH 5.5 and 278 K [42]. The NMR model structures of both peptides show, however, some deviations from the canonical 3 : 5 β-hairpin structure. To determine whether these deviations are present at the microscopic level or are a consequence of the conformational averaging inherent to the NMR experiment, four MD simulations in aqueous solution under various conditions have been performed for each of the two peptides (Table 1). The analysis of the simulations focuses on the study of β-hairpin stability and folding, and the

Table 1 Summary of the Simulations Performed

Peptide	Simulation	Starting structure	Temperature (K)	Number of atoms
10-residue	10_{β}^{278}	3 : 5 β-Hairpin (NMR[a])	278	5621
	10_{E}^{278}	Extended chain	278	13 865
	10_{E}^{323}	Extended chain	323	13 865
	10_{E}^{353}	Extended chain	353	13 865
15-residue	15_{β}^{278}	3 : 5 β-Hairpin (NMR[b])	278	7649
	$15_{\beta S}^{278}$	3 : 5 β-Hairpin (NMR[b]) 150 mM NaCl	278	7623
	$15_{\beta I}^{278}$	Canonical 3 : 5 β-hairpin	278	7649
	15_{α}^{278}	Canonical α-helix	278	7274

[a] NMR model structure with lowest energy in the structure calculation [40].
[b] NMR model structure with lowest energy in the structure calculation [39].

results are discussed within the context of the NMR data.

METHODS

MD Simulations

The simulations were carried out using the GROMOS96 package of programs [38,43].

The peptide model is as defined within the GROMOS96 43A1 force field [38]. In this force field the aliphatic carbon atoms are represented as united atoms [44], i.e. every CH_n ($n = 1, 2, 3$) group is represented as a single particle. The ionizable groups were set to their protonated or deprotonated state according to standard pK_a values of amino acids and a pH of 5.5. The SPC water model [45] was used as solvent.

Four simulations were set up for each of the two peptides. They are defined in Table 1 and differ in either initial conditions or temperature. For every system, the initial peptide structure was placed at the centre of a periodic truncated-octahedron box. The minimum distance from any peptide atom to the box wall was 1.4 nm in this initial configuration. The solvent was introduced into the box by using as a building block a cubic configuration of 216 equilibrated SPC water molecules. All water molecules with the oxygen atom lying within 0.23 nm of a non-hydrogen peptide atom were then removed. Truncated-octahedron periodic boundary conditions were applied from this point onward.

A steepest-descent energy minimization of the system was performed in order to relax the solvent configuration. The peptide atoms were positionally restrained using a harmonic interaction with a force constant of 250 kJ mol^{-1} nm^{-2}. Then, a steepest-descent energy minimization of the system without restraints was performed to eliminate any residual strain. The energy minimizations were terminated when the energy change per step became smaller than 0.1 kJ mol^{-1}.

A 30 ns molecular dynamics simulation at the chosen temperature and 1 atm was performed for each of the systems. The simulation $10_E{}^{353}$ was extended to 56 ns. In simulations $10_E{}^{278}$, $10_\beta{}^{278}$, $15_\beta{}^{278}$, $15_{\beta S}{}^{278}$ and $15_\alpha{}^{278}$ the initial velocities of the atoms were taken from a Maxwell-Boltzmann distribution at 100 K. The temperature of the system was kept at 100 K during the first 25 ps, and then raised to 190 K and to 278 K in successive 25 ps intervals. During this initial 75 ps in which the system temperature was increased, all peptide atoms were positionally restrained using a harmonic interaction with a force constant of 2500 kJ mol^{-1} nm^{-2}, relaxed to 250 kJ mol^{-1} nm^{-2} in the last 25 ps. In simulation $15_{\beta I}{}^{278}$ the same protocol was followed, but extending to 50 ps the initial equilibration at 100 K. During the first 100 ps of $15_{\beta I}{}^{278}$ the distances between selected backbone NH-CO pairs were restrained to an upper-bound hydrogen–oxygen distance of 0.23 nm with a force constant of 10^3 kJ mol^{-1} nm^{-2}, to obtain a starting structure that satisfied the hydrogen bonding of a canonical 3:5 β-hairpin. The temperature and the pressure were brought and maintained at the desired values by means of temperature and pressure baths [46]. Simulations $10_E{}^{323}$ and $10_E{}^{353}$ were started from the coordinates and velocities of the system at time 100 ps in simulation $10_E{}^{278}$, raising the temperature of the bath to 323 K and 353 K, respectively, in one step. In all cases, the temperature of the solute (peptide and ions) and the solvent were weakly coupled to independent baths with a relaxation time of 0.1 ps. The pressure of the system (calculated through a molecular virial) was weakly coupled to the pressure bath with isotropic scaling and a relaxation time of 0.5 ps. An estimated value of $4.575\ 10^{-4}$ kJ^{-1} mol nm^3 was taken for the isothermal compressibility of the system [38]. Bond lengths were constrained to ideal values [38] using the SHAKE algorithm [47] with a geometric tolerance of 10^{-4}. A time step for the leap-frog integration scheme of 2 fs was used.

The non-bonded interactions were evaluated by means of a twin-range method: The short-range van der Waals and electrostatic interactions were evaluated at every time step by using a charge-group pair list that was generated with a short-range cut-off radius of 0.8 nm. Longer range van der Waals and electrostatic interactions, i.e. between charge groups at a distance longer than the short range cut-off and shorter than a long range cut-off of 1.4 nm, were evaluated every five time steps, together with the pair-list updates, and were kept unchanged between these updates. The cut-off radii were applied to the centres of geometry of the solute charge groups and to the oxygen atoms of the water molecules. Interactions beyond the long range cut-off of 1.4 nm were taken into account by using a Poisson-Boltzmann reaction field correction, assuming an electrostatic continuum with the relative dielectric permittivity calculated for SPC water ($\varepsilon_2 = 54.0$) [48].

Analysis

Trajectory coordinates and energies were stored at 0.5 ps intervals and used for analysis. The energy of the system and the volume reach an equilibrium within tens of ps (data not shown). Given that the total length of the trajectories is three orders of magnitude longer, no initial period of time was discarded as equilibration for the calculation of trajectory averages.

Least-squares translational and rotational fitting of atomic coordinates and calculation of atom-positional root-mean-square differences (RMSD) was based on the N, H, C_α, C_β, C, O atoms of all but the *N*- and *C*-terminal residues of the peptides.

A conformational-clustering analysis was performed on a set of 6000 peptide structures (11 200 for $10_E{}^{353}$) taken at 5 ps intervals from the simulation, using the atom-positional RMSD as similarity criterion. An RMSD similarity cut-off of 0.12 nm was used to cluster the structures sampled by the decapeptide, which corresponds approximately to the maximum atom-positional RMSD between any pair of the 20 NMR model structures. On the same grounds, an RMSD similarity cut-off of 0.15 nm was used to cluster the structures sampled by the pentadecapeptide. The clustering algorithm has been described in previous studies of peptide dynamics [49]. The average lifetimes of particular conformers, corresponding to clusters of structures, were calculated from the time sequence of the sampling of clusters. Every time a particular cluster is abandoned the time that the peptide has spent in this cluster is saved, and used for the calculation of the average lifetime of the conformer.

Hydrogen bonds were calculated using a geometric criterion. A hydrogen bond was thus defined by a minimum donor-hydrogen-acceptor angle of 135° and a maximum hydrogen–acceptor distance of 0.27 nm. Hydrogen bond percentages were calculated on the entire set of structures taken at 0.5 ps intervals. Assignment of secondary structure was done with the program PROCHECK [50], according to the method of Kabsch and Sander [51], on structures taken at 10 ps intervals.

Interproton distances derived from the experimental NOE intensities were compared with the corresponding average effective interproton distances in the simulations. The latter were calculated by means of an $\langle r^{-6}\rangle^{-1/6}$ averaging the instantaneous distances r in structures taken at 0.5 ps intervals. For this comparison, only the distance restraints coming from the NOE intensities that are relevant for the determination of secondary (3 : 5 β-hairpin) structure were taken into account (see Tables 2 and 3). As already mentioned, in the GROMOS96 43A1 force field aliphatic hydrogen atoms were treated within a united-atom model. Interproton distances involving

Table 2 Medium- and Long-range NOEs Observed for the 10-residue Peptide in Aqueous Solution at 2 mM Concentration, pH 4.3, 278 K (H_2O/D_2O 9 : 1 by volume, ROESY, 200 ms mixing time) and pH 6.3, 274 K (D_2O, ROESY, 100 ms mixing time) [40] and NOE effective violations in simulations $10_\beta{}^{278}$ and $10_E{}^{353}$

^{1}H resonance in Residue *i*	Residue *j*	NOE intensity[d]	$\langle r^{-6}\rangle^{-1/6} - r_{NOE}$ (nm) $10_\beta{}^{278}$	$10_E{}^{353}$
[a]NH Y2	NH T10	m	−0.13	−0.01
[a]NH Y2	C_β H T10	w	−0.03	−0.04
[c]C_α H Y2	$C_{\zeta 3}$H W9	m	−0.13	0.02
[b]C_δ H Y2	C_β H T10	m	0.02	0.05
[b]C_δ H Y2	C_γ H_3 T10	m	−0.04	−0.04
[c]C_ε H Y2	C_α H N4	m	−0.17	−0.08
[b]C_ε H Y2	C_β H T10	w	−0.15	−0.05
[b]C_ε H Y2	C_γ H_3 T10	m	−0.02	0.01
[a]C_α H I3	C_α H W9	m	−0.13	−0.04
[a]C_α H I3	C_β H/$C_{\beta'}$H W9	w	−0.14	−0.14
[a]C_β H I3	C_α H W9	w	−0.06	−0.04
[b]C_β H I3	$C_{\varepsilon 3}$H W9	w	−0.06	−0.03
[b]C_β H I3	$C_{\eta 2}$H W9	vw	−0.18	0.04
[b]C_β H I3	$C_{\zeta 3}$H W9	vw	−0.17	−0.06
[b]C_γ H I3	NH S5	vw	−0.04	0.02

Table 2 (*Continued*)

^{1}H resonance in Residue *i*	Residue *j*	NOE intensity[d]	$10_\beta{}^{278}$	$\langle r^{-6}\rangle^{-1/6} - r_{NOE}$ (nm) $10_E{}^{353}$
[b]C_γ H I3	C_α H G7	m	−0.06	0.02
[b]C_γ H/$C_{\gamma'}$H I3	$C_{\varepsilon 3}$H W9	vw	−0.11	−0.04
[b]C_γ H/$C_{\gamma'}$H I3	$C_{\delta 1}$H W9	w	−0.16	−0.06
[b]$C_{\gamma'}$H I3	NH G7	vw	−0.08	0.13
[b]$C_{\gamma'}$H I3	$C_{\eta 2}$H W9	vw	−0.18	−0.01
[b]C_γ H_3 I3	NH S5	w	0.00	0.05
[b]C_γ H_3 I3	NH G7	w	−0.18	0.20
[b]C_γ H_3 I3	C_α H G7	m-s	−0.05	0.19
[b]C_γ H_3 I3	C_α H W9	w	−0.16	−0.11
[b]C_γ H_3 I3	$C_{\varepsilon 3}$H W9	w	−0.08	−0.03
[b]C_γ H_3 I3	$C_{\delta 1}$H W9	vw	−0.22	−0.12
[b]C_γ H_3 I3	$C_{\eta 2}$H W9	vw	−0.27	−0.09
[b]C_δ H_3 I3	NH S5	w	0.05	0.04
[b]C_δ H_3 I3	C_α H G7	m-s	−0.07	0.06
[b]C_δ H_3 I3	C_α H W9	w	−0.11	−0.05
[b]C_δ H_3 I3	$C_{\varepsilon 3}$H W9	m	0.09	0.13
[b]C_δ H_3 I3	$C_{\delta 1}$H W9	w	−0.19	0.00
[b]C_δ H_3 I3	$C_{\zeta 2}$H W9	m	−0.07	0.12
[b]C_δ H_3 I3	$C_{\zeta 3}$H W9	vw	−0.09	−0.02
[a]NH N4	NH G7	w	−0.03	0.09
[a]NH N4	NH T8	w-m	−0.08	0.03
[b]NH N4	C_γ H_3 T8	vw	−0.03	−0.01
[a]NH N4	C_α H W9	vw	−0.24	−0.21
[a]$C_{\beta'}$H N4	NH D6	w-m	−0.12	−0.11
[b]$C_{\beta'}$H N4	C_γ H_3 T8	w	−0.07	−0.15
[b]N_δ H N4	C_β H T8	w	−0.16	−0.06
[b]$N_{\delta'}$H N4	NH T8	w	−0.07	−0.11
[a]C_α H S5	NH G7	m	0.04	0.09
[a]NH D6	NH T8	w	−0.03	−0.02
[a]$C_{\beta'}$H D6	NH T8	m	−0.02	0.06
[b]$C_{\beta'}$H D6	C_γ H_3 T8	w	−0.05	0.00

[a] NOEs between backbone protons and NOEs between backbone and C_β protons.
[b] NOEs between side-chain protons corresponding to facing residues in the 3 : 5 β-hairpin and NOEs involving protons in the turn region not included in[a].
[c] Other NOEs of medium or strong intensity.
[d] The NOE intensities were evaluated qualitatively and used to obtain upper limit distance constraints: s (strong; $r_{NOE} \leq 0.30$ nm), m-s (medium-strong; $r_{NOE} \leq 0.35$ nm), m (medium; $r_{NOE} \leq 0.40$ nm), w-m (weak-medium; $r_{NOE} \leq 0.45$ nm), w (weak; $r_{NOE} \leq 0.50$ nm), and vw (very weak; $r_{NOE} \leq 0.55$ nm).

aliphatic hydrogen atoms were thus calculated by defining virtual (for CH_1 and pro-chiral CH_2) and pseudo (for non-stereospecific CH_2 and CH_3) atomic positions for these hydrogen atoms at the time of analysis. Pseudo atomic positions were also used in typically unresolved cases like, for example, the $C_\gamma H$ protons of valine or the $C_\delta H$ and $C_\varepsilon H$ protons of tyrosine [38]. For consistency, the aliphatic hydrogen atoms of the NMR model structures have been treated likewise when comparing the average interproton distances with those in the simulations.

RESULTS AND DISCUSSION

Ideal 3 : 5 β-Hairpins and NMR Model Structures for the 10-residue and 15-residue Peptides

The 20 structures with lowest energies calculated from distance and dihedral-angle restraints derived

Table 3 Medium and Long range NOEs Observed for the 15-residue Peptide in Aqueous Solution at 2 mM Concentration, pH 5.5, 278 K (H_2O/D_2O 9 : 1 by Volume and D_2O, NOESY, 200 ms mixing time) [39] and Effective Violations of the NOE Distances in Simulation $15_\beta{}^{278}$

^{1}H resonance in Residue *i*	Residue *j*	NOE intensity[d]	$\langle r^{-6}\rangle^{-1/6} - r_{NOE}$ (nm) $15_\beta{}^{278}$
[a]C_α H S3	C_α H V13	s	−0.09
[b]C_α H S3	C_γ $H_3/C_{\gamma'}H_3$ V13	m	−0.22
[c]C_β H/$C_{\beta'}$H S3	$C_{\varepsilon 3}$H W11	m	−0.15
[a]C_β H/$C_{\beta'}$H S3	C_α H V13	m	−0.09
[b]C_β H/$C_{\beta'}$H S3	C_γ $H_3/C_{\gamma'}H_3$ V13	m	−0.24
[a]NH Y4	NH T12	m	−0.10
[c]C_α H Y4	$C_{\zeta 3}$H W11	s	−0.05
[a]$C_{\beta'}$H Y4	C_β H T12	vw	−0.03
[b]C_δ H Y4	C_β H T12	w	−0.22
[b]C_δ H Y4	C_γ H_3 T12	m	0.01
[c]C_δ H Y4	C_γ H_3 T14	m	−0.16
[c]C_ε H Y4	C_α H N6	m	−0.08
[b]C_ε H Y4	C_β H T12	w-m	−0.27
[b]C_ε H Y4	C_γ H_3 T12	s	−0.10
[c]C_ε H Y4	C_γ H_3 T14	s	0.01
[a]C_α H I5	C_α H W11	s	−0.05
[a]C_α H I5	C_β H/$C_{\beta'}$H W11	w	−0.13
[a]C_β H I5	C_α H G9	w	0.09
[b]C_β H I5	$C_{\delta 1}$H W11	w	−0.14
[b]C_β H I5	$C_{\zeta 3}$H W11	w	−0.12
[b]C_β H I5	$C_{\zeta 2}$H W11	w	−0.19
[b]C_γ H_3 I5	NH G9	w	0.09
[b]$C_{\gamma\gamma'}$H I5	NH G9	w	−0.18
[b]C_γ H_3 I5	C_α H/$C_{\alpha'}$H G9	m	0.23
[b]$C_{\gamma\gamma'}$H I5	C_α H/$C_{\alpha'}$H G9	m	−0.05
[b]C_γ H_3 I5	C_α H W11	w-m	0.04
[b]$C_{\gamma\gamma'}$H I5	C_α H W11	w-m	−0.02
[b]C_γ H_3 I5	C_β H W11	vw	−0.02
[b]$C_{\gamma\gamma'}$H I5	C_β H W11	vw	−0.03
[b]C_γ H_3 I5	$C_{\delta 1}$H W11	m	0.11
[b]$C_{\gamma\gamma'}$H I5	$C_{\delta 1}$H W11	m	0.03
[b]C_γ H_3 I5	$C_{\varepsilon 3}$H W11	w	−0.03
[b]$C_{\gamma\gamma'}$H I5	$C_{\varepsilon 3}$H W11	w	0.06
[b]C_γ H_3 I5	$C_{\zeta 3}$H W11	w	−0.12
[b]$C_{\gamma\gamma'}$H I5	$C_{\zeta 3}$H W11	w	0.06
[b]C_γ H_3 I5	$C_{\zeta 2}$H W11	w	−0.20
[b]$C_{\gamma\gamma'}$H I5	$C_{\zeta 2}$H W11	w	−0.10
[b]C_δ H_3 I5	NH G9	w	−0.30
[b]C_δ H_3 I5	C_α H/$C_{\alpha'}$H G9	m	−0.18
[b]C_δ H_3 I5	C_α H W11	w	−0.19
[b]C_δ H_3 I5	$C_{\delta 1}$H W11	w-m	−0.19
[b]C_δ H_3 I5	$C_{\varepsilon 3}$H W11	vw	−0.06
[b]C_δ H_3 I5	$C_{\zeta 2}$H W11	s	0.04
[a]C_β H/$C_{\beta'}$H N6	NH T10	m	0.06
[b]C_β H N6	C_γ H_3 T10	w	−0.14
[a]$C_{\beta'}$H N6	NH D8	m	0.13
[a]NH D8	C_α H T10	w	0.23
[b]NH D8	C_γ H_3 T10	m	0.24
[a]C_α H D8	NH T10	w	−0.09
[b]C_β H D8	C_γ H_3 T10	w	−0.02
[c]C_β H/$C_{\beta'}$H W11	C_γ $H_3/C_{\gamma'}H_3$ V13	w-m	−0.03
[c]$C_{\delta 1}$H W11	C_γ $H_3/C_{\gamma'}H_3$ V13	m	0.43

[a] NOEs between backbone protons and NOEs between backbone and C_β protons.
[b] NOEs between side-chain protons corresponding to facing residues in the 3 : 5 β-hairpin and NOEs involving protons in the turn region not included in[a].
[c] Other NOEs of medium or strong intensity.
[d] The NOE intensities were evaluated qualitatively and used to obtain upper limit distance constraints: s (strong; $r_{NOE} \leq 0.30$ nm), m-s (medium-strong; $r_{NOE} \leq 0.35$ nm), m (medium; $r_{NOE} \leq 0.40$ nm), w-m (weak-medium; $r_{NOE} \leq 0.45$ nm), w (weak; $r_{NOE} \leq 0.50$ nm), and vw (very weak; $r_{NOE} \leq 0.55$ nm).

from experimental NMR parameters were considered as representative of the conformation adopted by the peptide in aqueous solution at 278 K [39,40]. The maximum atom-positional RMSD (see Methods) between the 20 NMR model structures is 0.12 nm for the decapeptide and 0.15 nm for the pentadecapeptide. These NMR structures conform to the basic description of a 3 : 5 β-hairpin with a type I + G1 β-bulge turn that is characterized by a three-residue turn and a single interstrand hydrogen bond between the residues flanking the turn [15–17], but show some deviations from the ideal hairpin structure.

For the 10-residue peptide SYINSDGTWT, the hydrogen bonds characteristic of an ideal 3 : 5 β-hairpin are 2NH-10O, 10NH-2O, 4NH-8O and 7NH-4O (Figure 1A). Of them, 2NH-10O, 10NH-2O and 4NH-8O are present in 5%, 80% and 100%, respectively, of the 20 model structures, while the turn hydrogen bond 7NH-4O is replaced by 7NH-5O (45% occurrence), which is also compatible with a I + G1 β-bulge turn conformation. For the 15-residue peptide SESYINSDGTWTVTE, the canonical

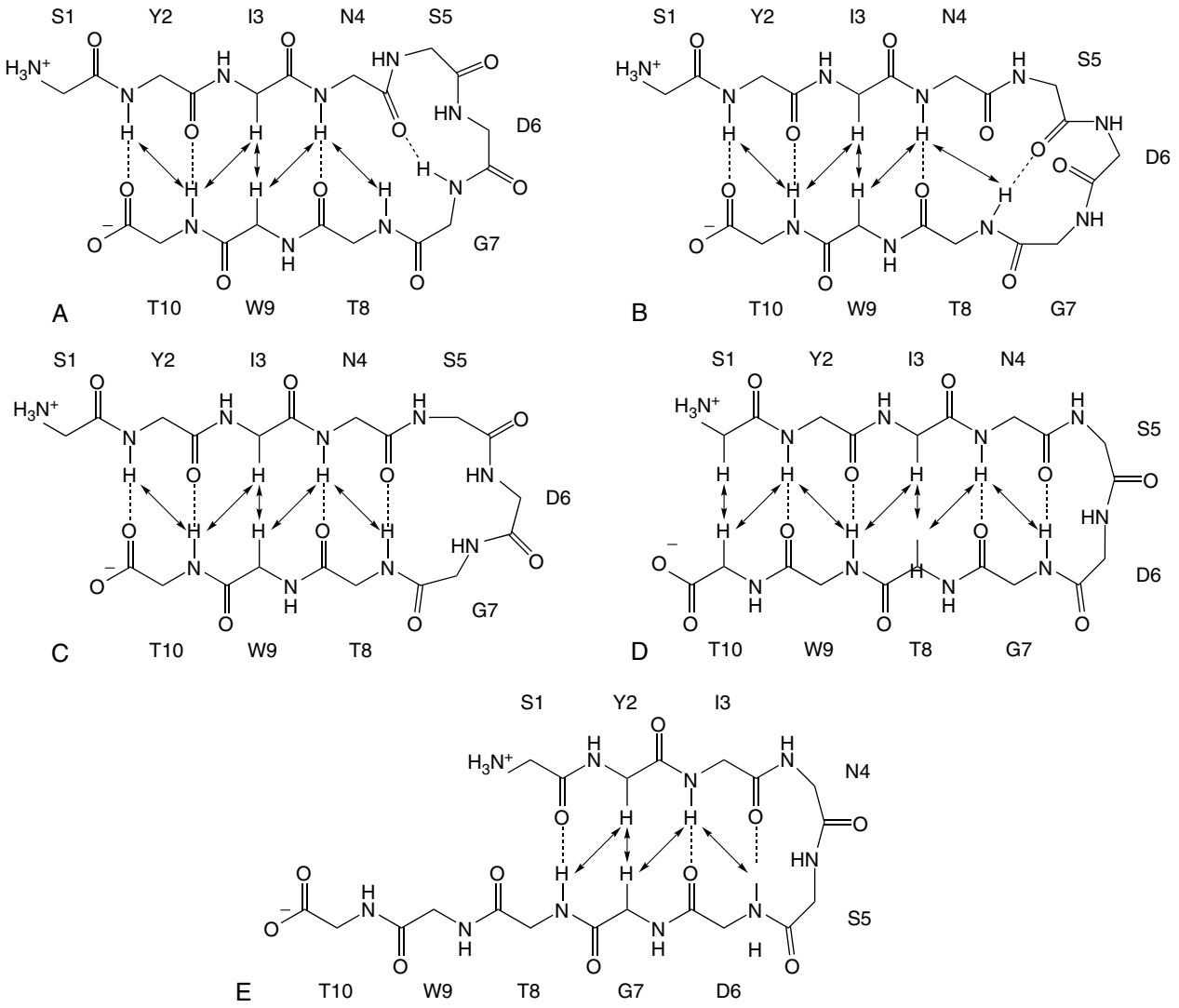

Figure 1 Backbone representation of β-hairpin conformations of the 10-residue peptide. A: 3:5 β-hairpin with a type I + G1 β-bulge turn; B: a variant of the 3:5 β-hairpin in A; C: 3:3 β-hairpin; D: 2:2 β-hairpin with a type I β-turn; E: 2:2 β-hairpin with a type I' β-turn. The double arrows indicate expected long-range NOEs between backbone protons. β-Sheet hydrogen bonds are indicated by dotted lines.

3:5 β-hairpin is defined by hydrogen bonds 2NH-14O, 14NH-2O, 4NH-12O, 12NH-4O, 6NH-10O and 9NH-6O (Figure 2A). Of those, only 14NH-2O and 6NH-10O are found in 5% and 55%, respectively, of the 20 model structures. In this case, the turn hydrogen bond, 9NH-6O, is also absent. The fact that the hydrogen bonds located at the peptide ends are absent or have a low occurrence may be consequence of a fraying effect, equivalent to that observed at the end of α-helices [6].

In line with the hydrogen bonding analysis, the program PROCHECK [50] recognizes only some of the structural features of ideal 3:5 β-hairpins in both sets of NMR model structures, that is, a β-bridge centred at residues 3 and 9 for 18 of the decapeptide structures, and a hydrogen-bonded turn involving residues 6 to 9 for 5 of the pentadecapeptide structures. PROCHECK assigns a β-bridge if there are two consecutive hydrogen bonds characteristic of a β-structure [51], e.g. 4NH-8O and 10NH-2O in the decapeptide.

Overall, the analysis of the NMR model structures indicates that both the decapeptide and the pentadecapeptide, and especially the latter, deviate from canonical 3:5 β-hairpin structures. At a microscopic level, this may have two, non-exclusive,

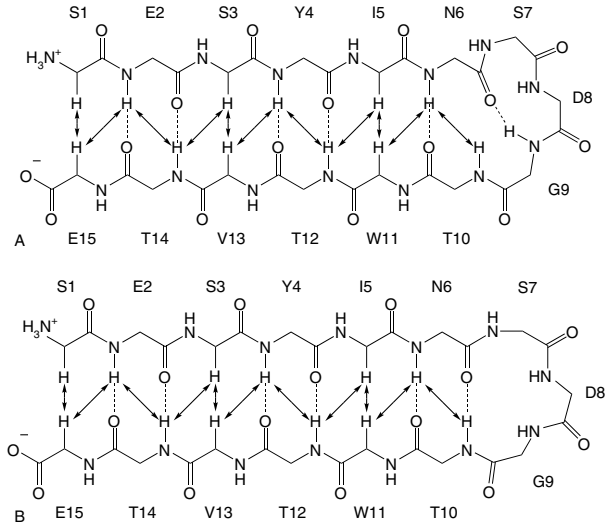

Figure 2 Backbone representation of β-hairpin conformations of the 15-residue peptide. A: 3:5 β-hairpin with a type I + G1 β-bulge turn; B: 3:3 β-hairpin. The double arrows indicate expected long-range NOEs between backbone protons. β-Sheet hydrogen bonds are indicated by dotted lines.

explanations: (i) the most stable structure is indeed a non-canonical β-hairpin; and (ii) the NMR data used in the structure calculation originate not only from an ideal 3:5 β-hairpin type of structure but also from other stable conformers such as non-canonical 3:3 or 3:5 β-hairpins (Figures 1 and 2). The simulations that will be presented below should provide the resolution that is necessary to answer this question.

β-Hairpin Stability in a Simulation of the 10-residue Peptide (10_β^{278})

A 30 ns MD simulation of the decapeptide, aimed at examining the stability of the 3:5 β-hairpin at 278 K, was performed starting from the lowest-energy NMR model structure (NMR structure 1). The time evolution of secondary structure assignment per residue, intramolecular hydrogen bonds and atom-positional RMSD from the initial structure is shown in Figure 3. The structure of the decapeptide fluctuates around the 3:5 β-hairpin conformation during the entire 30 ns trajectory: the β-bridge centred at residues 3 and 9 is almost continuously present along the simulation (Figure 3, upper panel) and the hydrogen bonds 2NH-10O (95% occurrence), 10NH-2O (87%) and 4NH-8O (74%) are present in a high percentage of the structures (Figure 3, middle panel). The turn region, with residues 5, 6 and 7, appears more structured than in the NMR model structures. The hydrogen bond 8NH-5O (11% occurrence) is predominant at this position in the first 11 ns of the simulation, while 7NH-4O (13%) is predominant in the next 19 ns. They are both compatible with a 3:5 β-hairpin (Figures 1B and 1A, respectively). In the interval from 4 to 11 ns the 3:5 β-hairpin alternates at times with a 3:3 β-hairpin (Figure 1C), in which the region of interstrand contact extends one position towards the turn with the hydrogen bond 8NH-4O (9% occurrence). This extension of the β-sheet is also apparent in the secondary structure analysis (Figure 3, upper panel). The hydrogen bond 8NH-4O has brief overlaps with 7NH-4O and with 8NH-5O at the turn.

The atom-positional RMSD from the initial structure of the decapeptide (NMR structure 1) is shown in the lower panel of Figure 3 as a function of time. Although the 3:5 β-hairpin conformation is well represented in the simulation, the atom-positional RMSD for the backbone atoms of residues 2 to 9 is never below 0.1 nm after the initial 0.2 ns and mostly over 0.12 nm, which is the maximum RMSD between any two NMR model structures. The rapid drift from the NMR structure without loss of the basic conformation is indicative of a relaxation process. This type of relaxation processes typically occurs when the experimental structure is strained, which is normally due to the presence of conflicting restraints. It could also be due to the protocol followed in the NMR structure calculation, which is based on distance-geometry calculations with the program DIANA [52] without subsequent restricted molecular dynamics.

A clustering analysis of structures extracted at 5 ps intervals from the trajectory shows that the canonical 3:5 β-hairpin is indeed the most populated conformer in the simulation. The central member structure of cluster number 1, corresponding to time 21.545 ns, is characterized by the hydrogen bonds 2NH-10O, 10NH-2O, 4NH-8O and 7NH-4O (Figure 4A). The percentage weight of this cluster in the ensemble is 55%, and the average lifetime of the conformer is 155 ps (with 105 visits). The central member structure of cluster number 2, corresponding to time 10.260 ns, contains the same interstrand hydrogen bonds but replaces the 7NH-4O hydrogen bond at the turn region by 8NH-5O. The percentage weight of this cluster in the ensemble is 26% and the average lifetime of the conformer 65 ps (with 120 visits). The total number of clusters is 22.

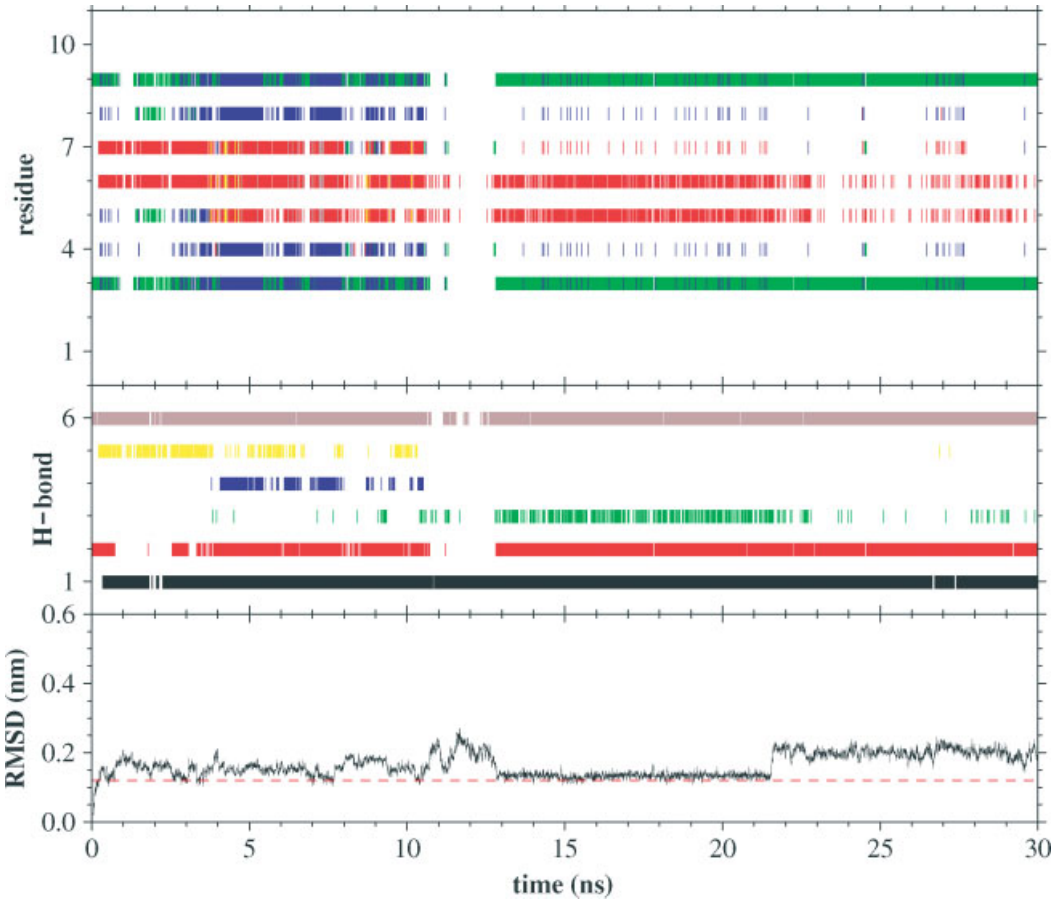

Figure 3 Structure as a function of time in simulation $10_{\beta}{}^{278}$. Upper panel: PROCHECK [50] secondary structure calculation. Red: hydrogen-bonded turn; yellow: 3_{10}-helix; brown: α-helix; green: β-bridge; blue: extended strand participating in β-ladder. Middle panel: Backbone hydrogen bonds with an occurrence in the simulation of 5% or more. 1: 2NH-10O (95% occurrence); 2: 4NH-8O (74% occurrence); 3: 7NH-4O (13% occurrence); 4: 8NH-4O (9% occurrence); 5: 8NH-5O (11% occurrence); 6: 10NH-2O (87% occurrence). Lower panel: Atom-positional root-mean-square deviation (RMSD) from the NMR structure 1 for the backbone atoms of residues 2–9. The red-dashed line indicates the maximum RMSD between any pair of the 20 NMR model structures (0.12 nm).

β-Hairpin Stability in Simulations of the 15-residue Peptide ($15_{\beta}{}^{278}$, $15_{\beta S}{}^{278}$, $15_{\beta I}{}^{278}$ and $15_{\alpha}{}^{278}$)

The stability of the 3:5 β-hairpin conformation of the pentadecapeptide was also examined from a 30 ns MD simulation, started from the lowest-energy NMR model structure (NMR structure 1) ($15_{\beta}{}^{278}$). The secondary structure and hydrogen bonding analyses (Figure 5, upper and middle panels, respectively) show that the peptide remains folded in a 3:5 β-hairpin conformation during the entire 30 ns trajectory. The β-bridged extended strands have a stable core involving residues 3–5 and 11–13, with temporary extensions on both sides of the ladder. The hydrogen bonds 14NH-2O (60% occurrence), 4NH-12O (95%), 12NH-4O (75%) and 6NH-10O (63%) are present in a high percentage of the structures. The comparatively low population of the terminal hydrogen bond, 2NH-14O (13% occurrence), may be caused by fraying of the peptide ends. The turn is characterized by the absence of the hydrogen bond 9NH-6O. Instead, 10NH-7O (35% occurrence) and 10NH-8O (15%), compatible with a 3:5 β-hairpin (Figure 2A), alternate in this region. At different times in the simulation the 3:5 β-hairpin inter-converts with a 3:3 β-hairpin (Figure 2B), in which the region of interstrand contact extends one position towards the turn with the hydrogen bond 10NH-6O (10% occurrence). This extension of the β-bridged strands, which occurred in a similar percentage in the decapeptide simulation, is also apparent in the secondary structure analysis

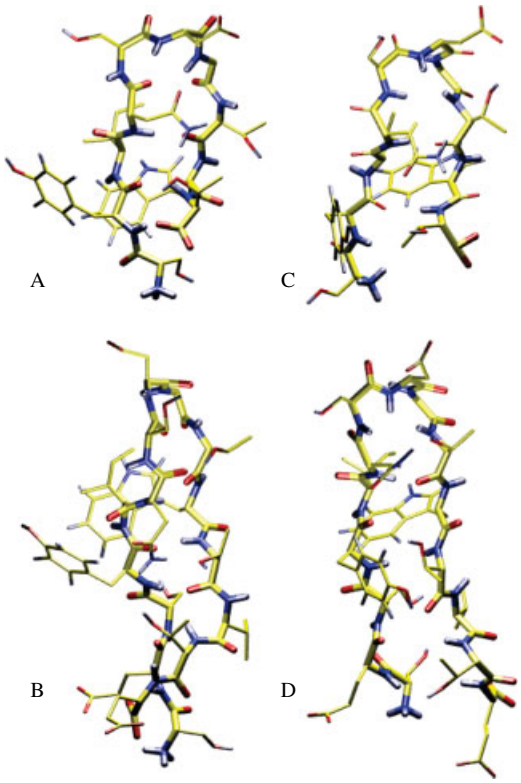

Figure 4 3:5 β-hairpin structures of the 10- and 15-residue peptides at 278 K. A: central member structure from cluster 1 in simulation 10_{β}^{278} (21.545 ns); B: central member structure from cluster 1 in simulation 15_{β}^{278} (25.820 ns); C: lowest-energy NMR model structure (NMR structure 1) for the decapeptide; D: lowest-energy NMR model structure (NMR structure 1) for the pentadecapeptide.

(Figure 5, upper panel). The hydrogen bond 10NH-6O has brief overlaps with 10NH-7O at the turn.

The atom-positional RMSD from the initial structure of the pentadecapeptide (NMR structure 1) is shown as a function of time in the lower panel of Figure 5. As observed for the decapeptide, even though the 3:5 β-hairpin conformation is well represented in the simulation, the atom-positional RMSD for the backbone atoms of residues 2–14 drifts rapidly to relatively high values. Thus, it is rarely below 0.15 nm (maximum RMSD between any two NMR model structures) after the initial 0.1 ns.

A clustering analysis of structures extracted at 5 ps intervals from the trajectory shows that the 3:5 β-hairpin is indeed the most populated conformer in the simulation. The central member structure of cluster number 1, corresponding to time 25.820 ns, is characterized by the hydrogen bonds 14NH-2O, 4NH-12O, 12NH-4O, 6NH-10O and 10NH-7O (Figure 4B). The hairpin has a pronounced twist in the direction of its long axis, which in this case is partly responsible for the relatively large RMSD from the NMR structure 1. This twist is also partially present in the central member structure of the most populated conformation of the decapeptide. The twist is apparently induced by the interactions between the side chains of Tyr, Ile and Trp at one face of the hairpin, which are in identical arrangement in the structures shown in Figures 4A and 4B. At the opposite face of the hairpin, the side chain of Asn interacts with Thr10 in the decapeptide and with Thr12 and Thr14 in the pentadecapeptide. This is in contrast to the situation in the NMR model structures, where the Trp side chain interacts with the Ile side chain at one face of the hairpin while the Tyr side chain interacts with Thr10 in the 10-residue peptide (Figure 4C), and Thr12 in the 15-residue peptide (Figure 4D). Nevertheless, the interaction of Tyr with Ile and Trp is also compatible with the upper-bound distances derived from the NOE intensities (see Tables 2 and 3).

The percentage weight of cluster 1 in the ensemble of conformers sampled for the pentadecapeptide is 96%. The average lifetime of the most populated conformer is 300 ps (with 75 visits). Cluster number 2 contains the conformation that corresponds to the NMR model structures. It alternates with cluster 1 during the first 6 ns of simulation. The total number of clusters is 6. The presence of such a small number of conformers in the clustering analysis indicates that the relative heterogeneity in the pattern of hydrogen bonds (Figure 5, middle panel) does not have a counterpart in RMSD space, that is, the structural fluctuations associated with the creation and destruction of some of the hydrogen bonds are small. The strand register characteristic of the 3:5 β-hairpin is also maintained in most cases.

The effect of the ionic species present in the experimental solution on the stability of the peptide was examined by means of a second 30 ns molecular dynamics simulation of the pentadecapeptide at 278 K with 150 mM NaCl ($15_{\beta S}^{278}$). In addition, a third 30 ns simulation at 278 K starting from a canonical 3:5 β-hairpin structure was performed to investigate the influence of the starting structure on the results ($15_{\beta I}^{278}$). In the latter case, the model was constructed by applying backbone hydrogen-bond distance restraints in a 100 ps MD simulation starting from the NMR structure 1 (see Methods). There is no significant difference between the trajectories sampled for the peptide in simulations 15_{β}^{278}, $15_{\beta S}^{278}$ and $15_{\beta I}^{278}$. This fact is illustrated

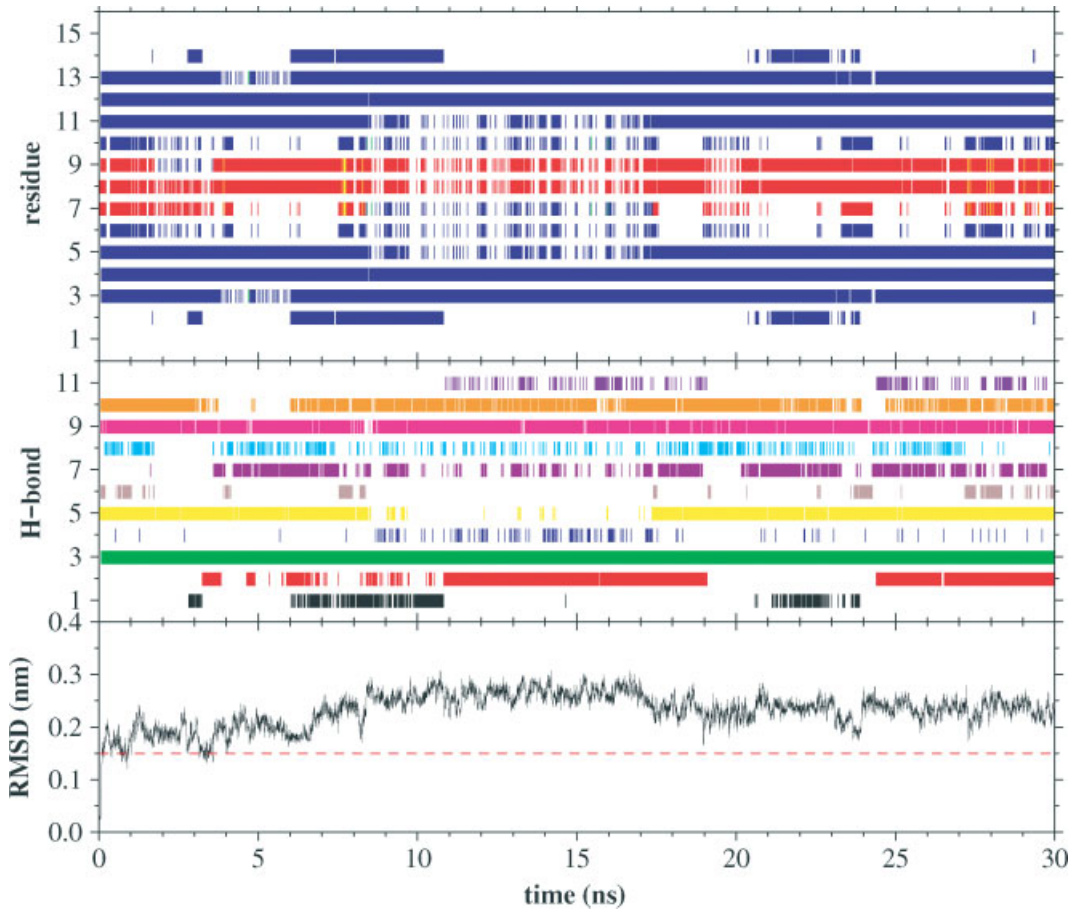

Figure 5 Structure as a function of time in simulation $15_{\beta}{}^{278}$. Upper panel: PROCHECK [50] secondary structure calculation. Red: hydrogen-bonded turn; yellow: 3_{10}-helix; brown: α-helix; green: β-bridge; blue: extended strand participating in β-ladder. Middle panel: Backbone hydrogen bonds with an occurrence in the simulation of 5% or more. 1: 2NH-14O (13% occurrence); 2: 2NH-15O (52% occurrence); 3: 4NH-12O (95% occurrence); 4: 6NH-4O (5% occurrence); 5: 6NH-10O (63% occurrence); 6: 10NH-6O (10% occurrence); 7: 10NH-7O (35% occurrence); 8: 10NH-8O (15% occurrence); 9: 12NH-4O (75% occurrence); 10: 14NH-2O (60% occurrence); 11: 15NH-2O (10% occurrence). Lower panel: Atom-positional root-mean-square deviation (RMSD) from the NMR structure 1 for the backbone atoms of residues 2–14. The red-dashed line indicates the maximum RMSD between any pair of the 20 NMR model structures (0.15 nm).

with Table 4, which shows the result of a clustering analysis on an ensemble of structures generated by concatenating the three trajectories. Thus, cluster number 1, which accounts for 89% of the total ensemble of 18 000 structures, contains a 36% of structures from $15_{\beta}{}^{278}$, a 30% of structures from $15_{\beta S}^{278}$ and a 34% of structures from $15_{\beta I}{}^{278}$. This overlap exists also in less populated clusters. The analysis data from simulations $15_{\beta S}^{278}$ and $15_{\beta I}{}^{278}$ are available upon request as supplementary material.

In order to investigate whether the stability of the β-hairpin at 278 K was not merely a consequence of the relatively short time scale explored, the same peptide sequence was built into an α-helix and a molecular dynamics simulation at the same temperature was performed (15_{α}^{278}). Within 30 ns of simulation more than half of the helix was lost. The unfolding starts at the *C*-terminus and progresses during 17 ns, until only the *N*-terminal hydrogen-bonded turn is left (between residues 2 and 6). This turn is then stable for the rest of the simulation. The analysis data from simulation 15_{α}^{278} are available upon request as supplementary material.

Comparison Between the Trajectories $10_{\beta}{}^{278}$ and $15_{\beta}{}^{278}$ and the Corresponding NMR Data

The upper-bound distances derived from the experimental NOE intensities (r_{NOE}) and the corresponding

Table 4 Clusters of Structures from a Trajectory Obtained by Concatenating the Trajectories 15_{β}^{278}, $15_{\beta S}^{278}$ and $15_{\beta I}^{278}$. A RMSD Similarity cut-off of 0.15 nm is used

Cluster no.	Total no. of elements	Elements from 15_{β}^{278} (%)	Elements from $15_{\beta S}^{278}$ (%)	Elements from $15_{\beta I}^{278}$ (%)	Weight in the ensemble (%)
1	16031	35.9	30.5	33.6	89.06
2	837	14.8	52.3	32.9	4.65
3	570	7.7	46.7	45.6	3.17
4	327	0.0	96.3	3.7	1.82
5	106	54.7	41.5	3.8	0.59
6	36	13.9	86.1	0.0	0.20
7	35	0.0	25.7	74.3	0.19
8	32	0.0	12.5	87.5	0.18
9	12	8.3	8.3	83.3	0.07
10	8	100.0	0.0	0.0	0.04
11	3	33.3	33.3	33.3	0.02
12	2	0.0	100.0	0.0	0.01
13	1	0.0	0.0	100.0	0.01

differences with the average effective distances calculated from the molecular dynamics trajectories ($\langle r^{-6}\rangle^{-1/6}$) are given in Table 2 for the decapeptide and Table 3 for the pentadecapeptide. For this analysis only the distance restraints derived from NOE intensities that are relevant for the determination of secondary (3 : 5 β-hairpin) structure were considered. Negative values of $\langle r^{-6}\rangle^{-1/6} - r_{NOE}$ may not be considered violations of the NOE-derived restraints. The trajectory from simulation 10_{β}^{278} is compatible with the upper-bound distances obtained for the decapeptide (Table 2). Only the average distance between the $C_{\delta}H_3$ group of Ile3 and the $C_{\varepsilon 3}H$ atom of Trp9 is in the simulation significantly (>0.05 nm) larger than the experimentally derived upper-bound. This distance is violated despite the close interaction between the two side chains in the conformer that is most populated in the simulation. Indeed, all other measured distances between the two side chains are within the experimental bounds.

The trajectory from simulation 15_{β}^{278} shows more discrepancies with the experimentally derived upper-bound distances (Table 3). Of 52 distances, there are five violations in the range 0.05 to 0.1 nm, two violations in the range 0.1 to 0.2 nm, three violations in the range 0.2 to 0.3 nm, and one violation larger than 0.4 nm. The violations in the range 0.2 to 0.3 nm involve residues at the β-turn. This might be an indication that the structural properties of the turn region are not sufficiently well represented in the 30 ns simulation. It should be noted that five of the violations larger than 0.05 nm correspond to distances derived from NOEs involving $C_{\gamma\gamma'}H$ or/and $C_{\gamma}H_3$ Ile protons whose assignment is ambiguous due to their chemical shift degeneracy [39]. In most cases, distance violations corresponding to simulations 15_{β}^{278}, $15_{\beta S}^{278}$ and $15_{\beta I}^{278}$ involved the same NOEs and their values are also very similar.

β-Hairpin Folding in Simulations of the 10-residue Peptide (10_E^{278}, 10_E^{323} and 10_E^{353})

To study the folding of the 10-residue peptide into the β-hairpin conformation, three molecular dynamics simulations starting from a fully extended conformation of the peptide (all backbone dihedral angles in *trans*) were performed at different temperatures. The simulations were carried out for 30 ns at 278 K (simulation 10_E^{278}), 30 ns at 323 K (simulation 10_E^{323}) and 56 ns at 353 K (simulation 10_E^{353}). 353 K is the highest temperature at which traces of a β-hairpin conformation could still be observed experimentally. Note, that the conformational space accessible to the peptide depends on the temperature of the system among other environment parameters. Moreover, the relative populations of particular conformations may change with increasing temperature. Therefore, the most stable or populated conformer at 278 K does not need to be the most populated at 353 K.

At 278 K the system has a low kinetic energy, and conformational transitions involving the crossing of relatively high energy barriers occur with

an accordingly low probability. Under these conditions, a 30 ns simulation proves to be far too short to observe the folding of the decapeptide from an extended chain into the 3 : 5 β-hairpin conformation. The peptide abandons rapidly the extended conformation to form, after 4 ns, a β-bridge involving residues 6 and 9. This conformer is dominant for the rest of the 30 ns, with a 17% occurrence of the 6NH-9O hydrogen bond and a 68% occurrence of 9NH-6O (supplementary material is available upon request). With the aim to shorten the time interval between conformational transitions, simulations at 323 K and 353 K were performed. The time evolution of secondary structure assignment per residue, intramolecular hydrogen bonds and atom-positional RMSD from the NMR structure 1 is shown in Figure 6 for simulation 10_E^{323} and Figure 7 for simulation 10_E^{353}.

At 323 K, the peptide adopts spontaneously a 2 : 2 β-hairpin with a type I β-turn (Figure 1D). The initiation of the hairpin conformation occurs early in the simulation (at around 2 ns) and the complete 2 : 2 β-hairpin is stable after 9 ns (Figure 6, upper panel). The structure of the peptide fluctuates around this conformation during the rest of the simulation. The central hydrogen bonds of the 2 : 2 β-hairpin, 9NH-2O (74% occurrence) and 4NH-7O (70%), are present in a high percentage of the structures (Figure 6, middle panel). The hydrogen bonds at the tail of the hairpin, 2NH-9O (21%

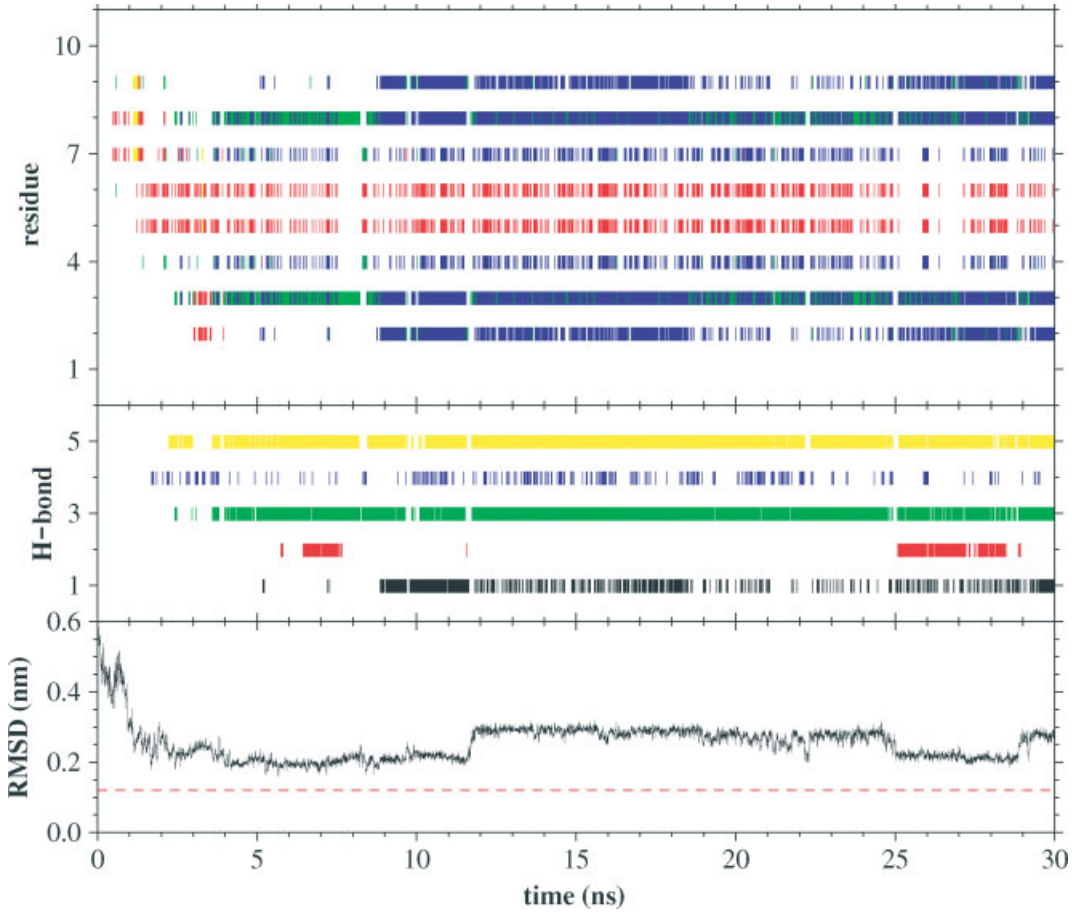

Figure 6 Structure as a function of time in simulation 10_E^{323}. Upper panel: PROCHECK [50] secondary structure calculation. Red: hydrogen-bonded turn; yellow: 3_{10}-helix; brown: α-helix; green: β-bridge; blue: extended strand participating in β-ladder. Middle panel: Backbone hydrogen bonds with an occurrence in the simulation of 5% or more. 1: 2NH-9O (21% occurrence); 2: 2NH-10O (12% occurrence); 3: 4NH-7O (70% occurrence); 4: 7NH-4O (10% occurrence); 5: 9NH-2O (74% occurrence). Lower panel: Atom-positional root-mean-square deviation (RMSD) from the NMR structure 1 for the backbone atoms of residues 2–9. The red-dashed line indicates the maximum RMSD between any pair of the 20 NMR model structures (0.12 nm).

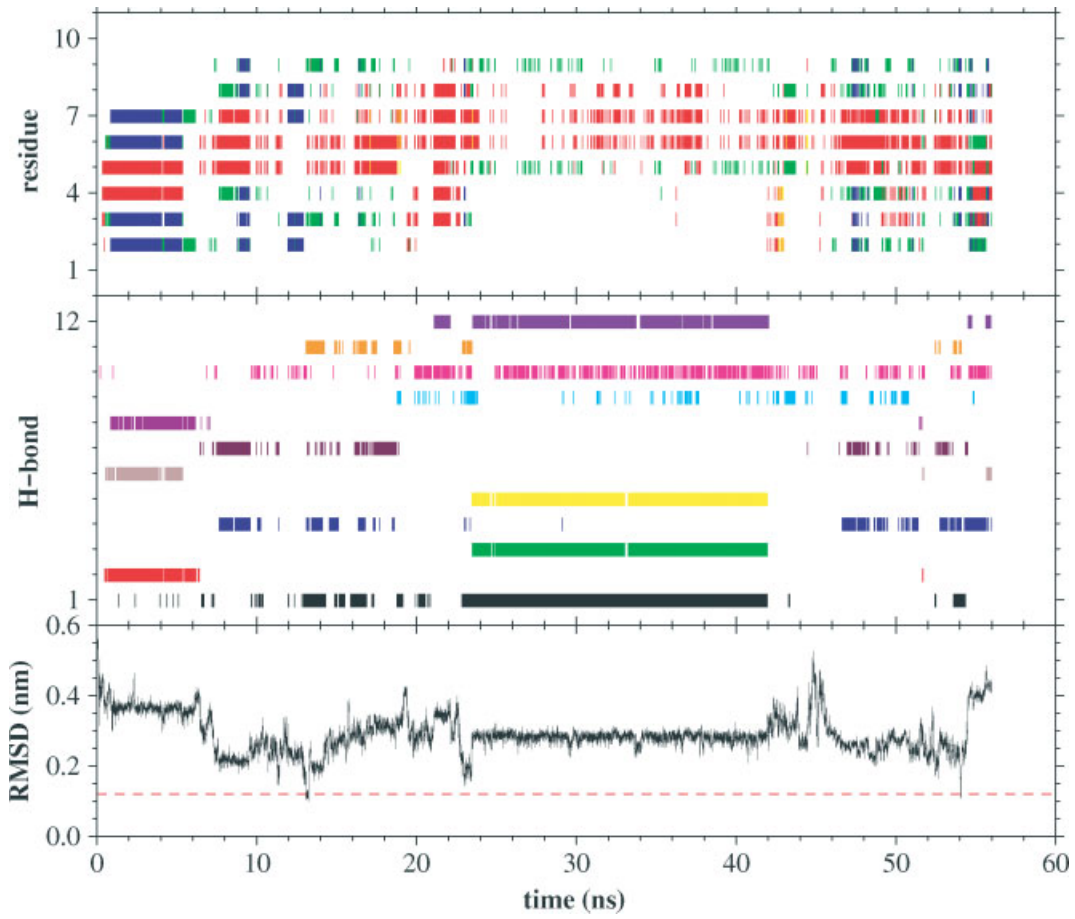

Figure 7 Structure as a function of time in simulation 10_E^{353}. Upper panel: PROCHECK [50] secondary structure calculation. Red: hydrogen-bonded turn; yellow: 3_{10}-helix; brown: α-helix; green: β-bridge; blue: extended strand participating in β-ladder. Middle panel: Backbone hydrogen bonds with an occurrence in the simulation of 5% or more. 1: 2NH-10O (41% occurrence); 2: 3NH-6O (8% occurrence); 3: 3NH-10O (28% occurrence); 4: 4NH-8O (12% occurrence); 5: 4NH-10O (30% occurrence); 6: 6NH-3O (5% occurrence); 7: 7NH-4O (7% occurrence); 8: 8NH-1O (5% occurrence); 9: 8NH-5O (5% occurrence); 10: 8NH-6O (13% occurrence); 11: 10NH-2O (5% occurrence); 12: 10NH-4O (24% occurrence). Lower panel: Atom-positional root-mean-square deviation (RMSD) from the NMR structure 1 for the backbone atoms of residues 2–9. The red-dashed line indicates the maximum RMSD between any pair of the 20 NMR model structures (0.12 nm).

occurrence), and at the turn region, 7NH-4O (10%), are less populated. The time sequence of the atom-positional RMSD from the NMR structure 1 (Figure 6, lower panel) shows that the 3 : 5 β-hairpin conformation has not been sampled even transiently. A clustering analysis of structures extracted at 5 ps intervals from the trajectory shows that the 2 : 2 β-hairpin is indeed the most populated conformer in the simulation. The central member structure of cluster number 1, corresponding to time 20.180 ns, is characterized by the hydrogen bonds 2NH-9O, 9NH-2O, 4NH-7O and 7NH-4O (Figure 8A). The percentage weight of this cluster in the ensemble is 48%, and the average lifetime of the conformer is 448 ps (with 30 visits). The central member structure of cluster number 2, corresponding to time 9.420 ns, contains only the core interstrand hydrogen bonds of the hairpin, 4NH-7O and 9NH-2O, which then is classified as a 2 : 4 β-hairpin. The percentage weight of this cluster in the ensemble is 30% and the average lifetime of the conformer 67 ps (with 134 visits). The total number of clusters is 70.

At 353 K, the peptide folds quickly (within 1 ns) from the extended structure to a 2 : 2 β-hairpin with a type I' β-turn (Figure 1E; upper panel of Figure 7). The presence of this conformation is determined

by the hydrogen bonds 8NH-1O (5% occurrence), 3NH-6O (8%) and 6NH-3O (5%) (Figure 7, middle panel). The 2:2 β-hairpin disappears 5 ns later, at about the same time that hydrogen bonds corresponding to a 3:5 β-hairpin start appearing. A completely structured 3:5 β-hairpin with a type I+G1 β-bulge turn is sampled for the first time at around 13 ns. Although this conformer shows reduced stability at 353 K, it is sampled at different times in the simulation, i.e. between 13 and 17 ns, at around 23 ns and at around 54 ns. The interstrand hydrogen bonds 2NH-10O, 10NH-2O and 4NH-8O are present in 41%, 5% and 12% of the structures, respectively. At the turn region, the hydrogen bond 7NH-4O (7% occurrence) is predominant, while 8NH-5O (5%) and 8NH-6O (13%) are scarce in the context of the 3:5 β-hairpin. The less stable 3:3 β-hairpin (Figure 1C, see the discussion on simulation 10_{β}^{278}), which contains the additional hydrogen bond 8NH-4O, is not sampled in simulation 10_{E}^{353}. Other conformations adopted by the peptide in this simulation, including the stable conformer visited in the interval from 24 to 42 ns, do not show particular secondary structure features. The atom-positional RMSD from the NMR structure 1 is plotted as a function of time in the lower panel of Figure 7. The three times that the 3:5 β-hairpin has been visited in the simulation can be roughly identified in this plot, although the 3:5 β-hairpin structures produced by the force field show some structural differences relative to the NMR model structure.

The conformation adopted by the peptide in the time interval from 24 to 42 ns constitutes the most populated cluster in a clustering analysis performed on 11 200 structures (1 per 5 ps). The central member structure of this cluster, corresponding to time 33.590 ns, is characterized by the hydrogen bonds 2NH-10O, 3NH-10O, 4NH-10O, 10NH-4O and 8NH-6O (Figure 8B). The β-bridge formed by the two hydrogen bonds between residues 4 and 10, and the two additional hydrogen bonds between residue 10 and residues 2 and 3, confer significant stability on this structure. The percentage weight of this cluster in the ensemble is 29%, and the average lifetime of the conformer is 98 ps (with 168 visits). The central member structure of cluster 2, corresponding to time 4.725 ns (Figure 8C), is a 2:2 β-hairpin with a type I' β-turn (Figure 1E). The percentage weight of this cluster in the ensemble is 8% and the average lifetime of the conformer 132 ps (with 34 visits). The 3:5 β-hairpin appears in clusters 6 and 17, with a total weight of 3%. The central member structure of cluster 6 (14.910 ns, Figure 8D) contains the hydrogen bonds 2NH-10O, 10NH-2O and 4NH-8O, while that of cluster 17 (23.075 ns) contains the hydrogen bonds 2NH-10O, 10NH-2O and the turn hydrogen bond 8NH-5O. The average lifetimes of the conformations represented by clusters 6 and 17 are 25 ps (with 51 visits) and 44 (with 11 visits), respectively. The total number of clusters from the 10_{E}^{353} trajectory is 357.

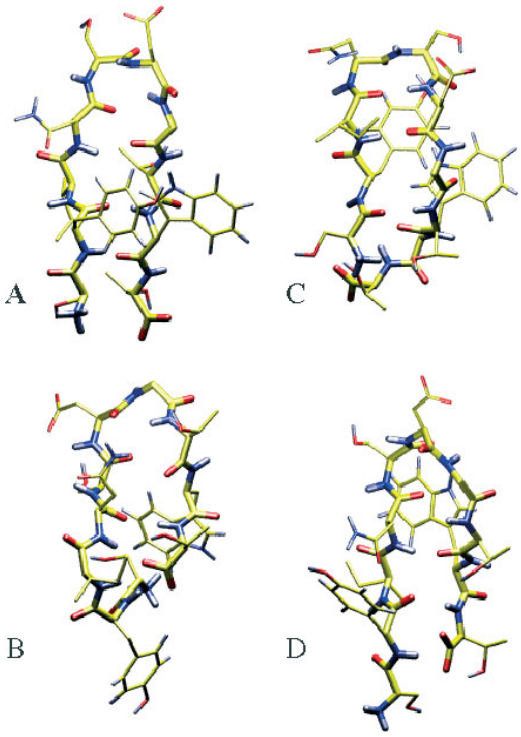

Figure 8 A: central member structure of cluster 1 from simulation 10_{E}^{323} (20.180 ns); B: central member structure of cluster 1 from simulation 10_{E}^{353} (33.590 ns); C: central member structure of cluster 2 from simulation 10_{E}^{353} (4.725 ns); D: central member structure of cluster 6 from simulation 10_{E}^{353} (14.910 ns).

The average effective interproton distances in simulations 10_{E}^{323} and 10_{E}^{353} are expected to violate a substantial number of the upper-bound distance restraints derived from the NOE intensities at 278 K (Table 2). This is clearly the case for simulation 10_{E}^{323}, where a type of β-hairpin different to that determined at 278 K dominates the trajectory. Surprisingly, the average distances from simulation 10_{E}^{353} are still in moderate agreement with the upper-bound distances. Thus, of the 46 experimentally derived distances shown in Table 2, there are only nine violations larger than 0.05 nm. This suggests that, despite the clearly insufficient time scale of the simulation, basic features of the

conformational behaviour of the peptide at 353 K are captured in the simulation.

β-Hairpin Folding Mechanism for the 10-residue Peptide at 353 K

In simulation 10_E^{353} the decapeptide samples a distribution of conformations including the 3:5 β-hairpin. By mapping the conformational space sampled onto a graph of transitions between clusters of structures (Figure 9), the most probable pathways of folding to a given conformer (cluster) can be delineated (Figure 10).

The graph shown in Figure 9 has been generated by connecting pairs of clusters (starting from cluster 1 and its neighbours) for which at least two transitions in each direction occur in simulation 10_E^{353}. Four families of conformers can be distinguished in this graph, dominated by clusters 1, 2, 3/6 and 4/5, respectively, with clusters 9 and 13 acting as unique connection points between them. The four families correspond to loop structures, with different degrees of β-hairpin character.

A simplified graph, giving structural information on key clusters along pathways between families, is shown in Figure 10. The initial collapse to a loop shape is very fast, and regions of conformational space corresponding to other types of ordered structures (e.g. helices) are never sampled. As already mentioned, the most stable structure of the decapeptide at this temperature (cluster 1) is a loop structure with a big number of backbone hydrogen bonds (Figures 8B and 10). Transitions from this cluster to the other three families of clusters require the loss of all these hydrogen bonds. Thus, cluster 9 corresponds to a sort of pluripotent loop structure characterized (and probably stabilized) by a single interstrand interaction between the side chains of Tyr2 and Trp9. This conformation may evolve to a different, yet unstructured, loop structure (cluster 13) or to a loop structure characterized by the hydrogen bonds 3NH-8O and 4NH-8O (cluster 31). In both cases the Tyr2-Trp9 side-chain interaction is conserved. From cluster 31 the peptide can access clusters 4 and 5, which preserve the 3NH-8O and 4NH-8O hydrogen bonds. The turn region of the conformer represented by cluster 4 belongs

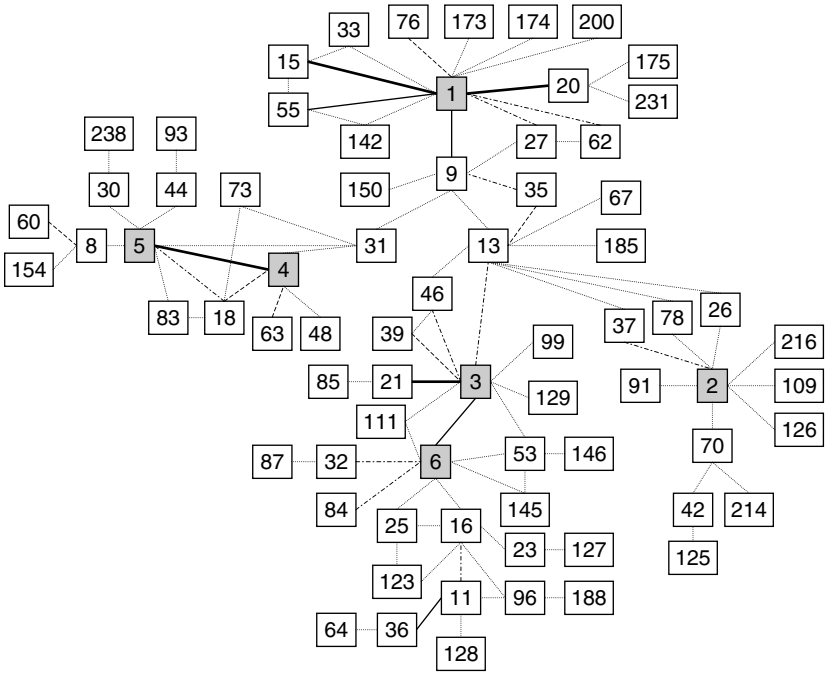

Figure 9 Graph of transitions between clusters of structures in simulation 10_E^{353}. Clusters are represented by boxes containing the cluster number. Only those transitions (connector between two clusters) that have been sampled at least twice in each direction in the simulation are shown. The average (from the two directions) number of transitions is indicated by a line code. Dotted line: 2–5 transitions; dot-dashed line: 6–10 transitions; dashed line: 11–15 transitions; thin-solid line: 16–20 transitions; thick-solid line: more than 20 transitions. The most populated clusters in each of the four families or branches of the graph (clusters 1, 2, 3/6, and 4/5) are coloured grey.

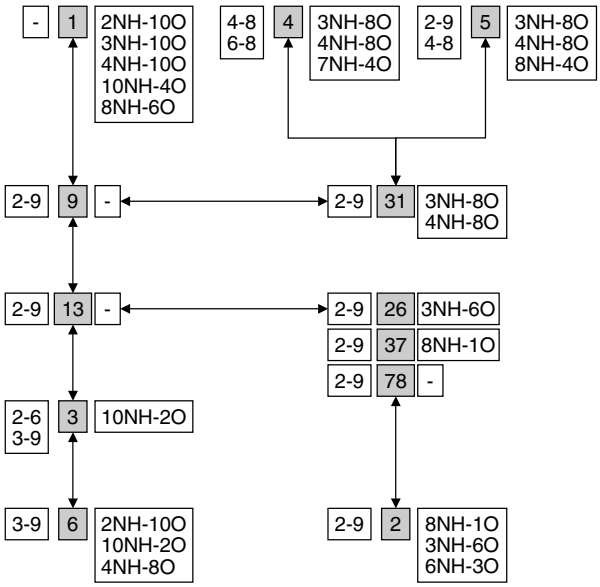

Figure 10 Simplified representation of main pathways between the most populated clusters in simulation $10_E{}^{353}$ (see Figure 9). Clusters are represented by grey boxes containing the cluster number. The box at the left of the cluster number enumerates side chain interactions which are conserved in the corresponding cluster. For example, 2–9 indicates that the side chains of Tyr2 and Trp9 are within direct-interaction distance in at least 50% of the structures in the cluster (side chains were not included in the clustering RMSD criterion). The box at the right of the cluster number enumerates the backbone hydrogen bonds. Hydrogen bonds involving residues Ser1 and Thr10 have been considered if they are present in at least 50% of the structures in the cluster (these residues were not included in the clustering RMSD criterion).

to a 3:5 β-hairpin with a I+G1 β-bulge turn, while that of cluster 5 belongs to a 3:3 β-hairpin. From cluster 13 the peptide can progress to two other families of conformers. In one of them, the side-chain interaction between Tyr2 and Trp9 is maintained and the structure evolves towards a 2:2 β-hairpin (cluster 2). In the other, the Tyr2–Trp9 side-chain interaction is broken to establish an Ile3–Trp9 interaction, and the structure evolves towards a 3:5 β-hairpin (cluster 6).

CONCLUSIONS

The dynamics of the 10-residue peptide SYINSDGTWT and the 15-residue peptide SESYINSDGTWTVTE under different conditions have been investigated by molecular dynamics simulation. The 3:5 β-hairpin conformations derived from NMR data at 278 K are stable over 30 ns simulations at this temperature, although some differences exist between the NMR model structures and the β-hairpin structures sampled in the simulations. For the 15-residue peptide, the stability of the β-hairpin proved to be independent of the particular structure used to start the simulation (NMR model or canonical 3:5 β-hairpin) and the absence or presence of salt in the solution (these tests were not performed for the decapeptide). The supposed stabilization of the β-hairpin conformation upon strand lengthening (i.e. from the 10-residue to the 15-residue peptide) is not evident in the simulations. Nevertheless, a comparison of stability from independent simulations is only feasible for large stability differences or very long simulation times. The average interproton distances calculated from the trajectories at 278 K satisfy the upper bounds derived from the NOE intensities, with the exception of some distances corresponding to the turn region of the 3:5 β-hairpin conformation of the 15-residue peptide.

To study the folding of the decapeptide, simulations at 278 K, 323 K and 353 K starting from an extended structure have been also performed. 30 ns were insufficient to observe folding to the 3:5 β-hairpin conformation at 278 K and 323 K. Interestingly, at 323 K the peptide adopted a stable 2:2 β-hairpin with a type I β-turn. This type of β-hairpin is not compatible with the NMR data at 278 K. At 353 K the conformational transitions occur at a sufficiently high rate that several events of folding to a 3:5 β-hairpin could be observed along a 56 ns simulation. This temperature was chosen for being the highest at which the NMR spectra were still indicative of a small population of 3:5 β-hairpin.

In the simulation of the 10-residue peptide at 353 K (and possibly more generally) the problem of β-hairpin folding is not that of evolving from an extended or random conformation to a specific type of β-hairpin, but that of moving towards a specific type of β-hairpin in a region of conformational space that is dominated by loop (or even β-hairpin) structures. The initial collapse to a loop shape is very fast, and regions of conformational space corresponding to other types of ordered structures (e.g. helices) are never sampled. This mechanism is compatible with previous experimental results on β-hairpin-forming peptides [53], indicating that the bending propensity of the turn segment drives the first steps of folding to a β-hairpin structure. Transitions between different types of loop and β-hairpin conformations occur

through two unstructured loop conformations, represented by clusters 9 and 13 (see Results and Discussion), that can easily evolve from and to different types of β-hairpin registers. The residues Tyr2 and Trp9 might play an important role in reducing the accessible conformational space to that of loop structures and in controlling the folding towards different types of β-hairpin structures (e.g. Tyr2–Trp9 in the path to the 2:2 β-hairpin, Ile3–Trp9 in the last steps of the path to the 3:5 β-hairpin). In this scenario, the fine organization of the turn region (with hydrogen bonds) occurs only towards the last steps of β-hairpin folding (see Figure 10).

The folding mechanism sketched above shares some key features with mechanisms of β-hairpin folding derived from previous simulation studies. Thus, initiation of β-hairpin folding by turn or loop formation has been observed for other β-hairpin forming peptides [30,35,54] as well as for small three-stranded β-sheet forming peptides [31,33,36]. Switching between different types of β-hairpin registers has also been observed in previous simulations of β-hairpin folding [35]. Finally, interactions among hydrophobic side chains have been found to be important for β-hairpin folding, and in some cases even proposed to be the initial driving force [26–29,32].

Experimental kinetic models suggest that β-hairpin folding occurs, in general, on the microsecond timescale [18,55]. The results reported here indicate, on the other hand, that the SYINSDGTWT peptide may fold on the nanosecond timescale (more precisely 10^{-8} s) at 353 K. There are a number of possible reasons for this apparent kinetic mismatch, none of them being *a priori* discardable:

1. Folding of the SYINSDGTWT peptide has been only observed in a simulation at 353 K. Compared with room temperature (or 278 K in the NMR experiment) the stability of the 3:5 β-hairpin conformation at 353 K decreases greatly, with an average lifetime in the subnanosecond timescale [56], i.e. below experimental resolution. At the same time, the frequency of sampling of the β-hairpin increases as a consequence of the faster transitions between conformers at high temperature. The kinetics of folding from simulation and experiment may not be directly comparable under these conditions.
2. A general timescale may not apply: β-hairpin folding kinetics might not only be strongly dependent on temperature and molecular environment, but also on sequence and chain length.
3. The computational model (force field and simulation methodology) may not be sufficiently good to reproduce the folding kinetics accurately.
4. The experimental resolution may not be sufficient to produce an accurate model for the kinetics of folding of small peptides. In order to describe the dynamics of a system in the 10^{-9}–10^{-8} s timescale, a technique with 10^{-11}–10^{-10} s resolution is required. Current techniques, e.g. laser temperature jump, have a resolution $\sim 10^{-8}$ s and are adequate for processes on the $\sim 10^{-6}$ s timescale. In addition, the interpretation (modelling) of the experimental data may be inadequate.

Acknowledgements

Financial support was obtained from the Schweizer Nationalfonds, project number 2000-063590.00, the Spanish DGYCT, project no. PB98-0677, and the European project CEE B104-97-2086, which are gratefully acknowledged. C. M. S. was recipient of a pre-doctoral fellowship from the Autonomous Community of Madrid, Spain.

REFERENCES

1. MacPhee CE, Dobson CM. Chemical dissection and reassembly of amyloid fibrils formed by a peptide fragment of transthyretin. *J. Mol. Biol.* 2000; **297**: 1203–1215.
2. Dobson CM. The structural basis of protein folding and its links with human disease. *Philos. Trans. R. Soc. Lond. Ser. B-Biol. Sci.* 2001; **356**: 133–145.
3. Scholtz JM, Baldwin RL. The mechanism of α-helix formation by peptides. *Annu. Rev. Biophys. Biomolec. Struct.* 1992; **21**: 95–118.
4. Lyu PC, Wemmer DE, Zhou HX, Pinker RJ, Kallenbach NR. Capping interactions in isolated α-helices: Position- dependent substitution effects and structure of a serine-capped peptide helix. *Biochemistry* 1993; **32**: 421–425.
5. Zhou NE, Kay CM, Sykes BD, Hodges RS. A single-stranded amphipathic α-helix in aqueous-solution: Design, structural characterization, and its application for determining α-helical propensities of amino-acids. *Biochemistry* 1993; **32**: 6190–6197.
6. Baldwin RL. α-Helix formation by peptides of defined sequence. *Biophys. Chem.* 1995; **55**: 127–135.
7. Muñoz V, Serrano L. Development of the multiple sequence approximation within the AGADIR model of α-helix formation: Comparison with Zimm-Bragg

and Lifson-Roig formalisms. *Biopolymers* 1997; **41**: 495–509.
8. Aurora R, Rose GD. Helix capping. *Protein Sci.* 1998; **7**: 21–38.
9. Smith CK, Regan L. Construction and design of β-sheets. *Acc. Chem. Res.* 1997; **30**: 153–161.
10. Blanco F, Ramírez-Alvarado M, Serrano L. Formation and stability of β-hairpin structures in polypeptides. *Curr. Opin. Struct. Biol.* 1998; **8**: 107–111.
11. Gellman SH. Minimal model systems for β-sheet secondary structure in proteins. *Curr. Opin. Chem. Biol.* 1998; **2**: 717–725.
12. Lacroix E, Kortemme T, de la Paz ML, Serrano L. The design of linear peptides that fold as monomeric β-sheet structures. *Curr. Opin. Struct. Biol.* 1999; **9**: 487–493.
13. Serrano L. The relationship between sequence and structure in elementary folding units. *Adv. Prot. Chem.* 2000; **53**: 49–85.
14. Venkatraman J, Shankaramma SC, Balaram P. Design of folded peptides. *Chem. Rev.* 2001; **101**: 3131–3152.
15. Sibanda BL, Thornton JM. β-Hairpin families in globular-proteins. *Nature* 1985; **316**: 170–174.
16. Sibanda BL, Blundell TL, Thornton JM. Conformation of β-hairpins in protein structures. A systematic classification with applications to modeling by homology, electron-density fitting and protein engineering. *J. Mol. Biol.* 1989; **206**: 759–777.
17. Sibanda BL, Thornton JM. Conformation of β-hairpins in protein structures. Classification and diversity in homologous structures. *Methods Enzymol.* 1991; **202**: 59–82.
18. Muñoz V, Thompson PA, Hofrichter J, Eaton WA. Folding dynamics and mechanism of β-hairpin formation. *Nature* 1997; **390**: 196–199.
19. Daura X, Jaun B, Seebach D, van Gunsteren WF, Mark AE. Reversible peptide folding in solution by molecular dynamics simulation. *J. Mol. Biol.* 1998; **280**: 925–932.
20. Duan Y, Kollman PA. Pathways to a protein folding intermediate observed in a 1- microsecond simulation in aqueous solution. *Science* 1998; **282**: 740–744.
21. Schäfer M, Bartels C, Karplus M. Solution conformations and thermodynamics of structured peptides: Molecular dynamics simulation with an implicit solvation model. *J. Mol. Biol.* 1998; **284**: 835–848.
22. Takano M, Yamato T, Higo J, Suyama A, Nagayama K. Molecular dynamics of a 15-residue poly(L-alanine) in water: Helix formation and energetics. *J. Am. Chem. Soc.* 1999; **121**: 605–612.
23. Hummer G, Garcia AE, Garde S. Helix nucleation kinetics from molecular simulations in explicit solvent. *Proteins: Struct. Funct. Genet.* 2001; **42**: 77–84.
24. Simmerling C, Strockbine B, Roitberg AE. All-atom structure prediction and folding simulations of a stable protein. *J. Am. Chem. Soc.* 2002; **124**: 11 258–11 259.
25. Snow CD, Nguyen H, Pande VS, Gruebele M. Absolute comparison of simulated and experimental protein-folding dynamics. *Nature* 2002; **420**: 102–106.
26. Prévost M, Ortmans I. Refolding simulations of an isolated fragment of barnase into a native-like β-hairpin: Evidence for compactness and hydrogen bonding as concurrent stabilizing factors. *Proteins: Struct. Funct. Genet.* 1997; **29**: 212–227.
27. Dinner AR, Lazaridis T, Karplus M. Understanding β-hairpin formation. *Proc. Natl Acad. Sci. USA* 1999; **96**: 9068–9073.
28. Pande VS, Rokhsar DS. Molecular dynamics simulations of unfolding and refolding of a β-hairpin fragment of protein G. *Proc. Natl Acad. Sci. USA* 1999; **96**: 9062–9067.
29. Roccatano D, Amadei A, Di Nola A, Berendsen HJ. A molecular dynamics study of the 41–56 β-hairpin from B1 domain of protein G. *Protein Sci.* 1999; **8**: 2130–2143.
30. Bonvin AMJJ, van Gunsteren WF. β-Hairpin stability and folding: Molecular dynamics studies of the first β-hairpin of tendamistat. *J. Mol. Biol.* 2000; **296**: 255–268.
31. Ferrara P, Caflisch A. Folding simulations of a three-stranded antiparallel β-sheet peptide. *Proc. Natl Acad. Sci. USA* 2000; **97**: 10 780–10 785.
32. Ma BY, Nussinov R. Molecular dynamics simulations of a β-hairpin fragment of protein G: Balance between side-chain and backbone forces. *J. Mol. Biol.* 2000; **296**: 1091–1104.
33. Wang HW, Sung SS. Molecular dynamics simulations of three-strand β-sheet folding. *J. Am. Chem. Soc.* 2000; **122**: 1999–2009.
34. Daura X, Gademann K, Schäfer H, Jaun B, Seebach D, van Gunsteren WF. The β-peptide hairpin in solution: Conformational study of a β-hexapeptide in methanol by NMR spectroscopy and MD simulation. *J. Am. Chem. Soc.* 2001; **123**: 2393–2404.
35. Higo J, Galzitskaya OV, Ono S, Nakamura H. Energy landscape of a β-hairpin peptide in explicit water studied by multicanonical molecular dynamics. *Chem. Phys. Lett.* 2001; **337**: 169–175.
36. Colombo G, Roccatano D, Mark AE. Folding and stability of the three-stranded β-sheet peptide Betanova: insights from molecular dynamics simulations. *Proteins: Struct. Funct. Genet.* 2002; **46**: 380–392.
37. Wu X, Wang S, Brooks BR. Direct observation of the folding and unfolding of a β-hairpin in explicit water through computer simulation. *J. Am. Chem. Soc.* 2002; **124**: 5282–5283.
38. van Gunsteren WF, Billeter SR, Eising AA, Hünenberger PH, Krüger P, Mark AE, Scott WRP, Tironi IG. *Biomolecular Simulation: The GROMOS96 Manual and User Guide*. vdf Hochschulverlag AG an der ETH Zürich and BIOMOS b.v: Zürich, Groningen 1996.

39. Santiveri CM, Rico M, Jiménez MA. Position effect of cross-strand side-chain interactions on β-hairpin formation. *Protein Sci.* 2000; **9**: 2151–2160.
40. de Alba E, Rico M, Jiménez MA. Cross-strand side-chain interactions versus turn conformation in β-hairpins. *Protein Sci.* 1997; **6**: 2548–2560.
41. Stanger HE, Syud FA, Espinosa JF, Giriat I, Muir T, Gellman SH. Length-dependent stability and strand length limits in antiparallel β-sheet secondary structure. *Proc. Natl Acad. Sci. USA* 2001; **98**: 12 015–12 020.
42. Santiveri CM, Rico M, Jimenez MA. $^{13}C_{\alpha}$ and $^{13}C_{\beta}$ chemical shifts as a tool to delineate β-hairpin structures in peptides. *J. Biomol. NMR* 2001; **19**: 331–345.
43. Scott WRP, Hünenberger PH, Tironi IG, Mark AE, Billeter SR, Fennen J, Torda AE, Huber T, Krüger P, van Gunsteren WF. The GROMOS biomolecular simulation program package. *J. Phys. Chem. A* 1999; **103**: 3596–3607.
44. Daura X, Mark AE, van Gunsteren WF. Parametrization of aliphatic CH_n united atoms of GROMOS96 force field. *J. Comput. Chem.* 1998; **19**: 535–547.
45. Berendsen HJC, Postma JPM, van Gunsteren WF, Hermans J. Interaction models for water in relation to protein hydration. In *Intermolecular Forces*, Pullman B (ed.). D. Reidel: Dordrecht 1981; 331–342.
46. Berendsen HJC, Postma JPM, van Gunsteren WF, Dinola A, Haak JR. Molecular dynamics with coupling to an external bath. *J. Chem. Phys.* 1984; **81**: 3684–3690.
47. Ryckaert JP, Ciccotti G, Berendsen HJC. Numerical integration of Cartesian equations of motion of a system with constraints: Molecular dynamics of n-alkanes. *J. Comput. Phys.* 1977; **23**: 327–341.
48. Smith PE, van Gunsteren WF. Consistent dielectric properties of the simple point-charge and extended simple point-charge water models at 277 and 300K. *J. Chem. Phys.* 1994; **100**: 3169–3174.
49. Daura X, van Gunsteren WF, Mark AE. Folding-unfolding thermodynamics of a β-heptapeptide from equilibrium simulations. *Proteins: Struct. Funct. Genet.* 1999; **34**: 269–280.
50. Laskowski RA, Macarthur MW, Moss DS, Thornton JM. PROCHECK — a program to check the stereochemical quality of protein structures. *J. Appl. Crystallogr.* 1993; **26**: 283–291.
51. Kabsch W, Sander C. Dictionary of protein secondary structure: pattern-recognition of hydrogen-bonded and geometrical features. *Biopolymers* 1983; **22**: 2577–2637.
52. Güntert P, Braun W, Wüthrich K. Efficient computation of three-dimensional protein structures in solution from nuclear magnetic resonance data using the program DIANA and the supporting programs CALIBA, HABAS and GLOMSA. *J. Mol. Biol.* 1991; **217**: 517–530.
53. Santiveri CM, Santoro J, Rico M, Jiménez MA. Thermodynamic analysis of β-hairpin-forming Peptides from the thermal dependence of ^{1}H NMR chemical shifts. *J. Am. Chem. Soc.* 2002; **124**: 14 903–14 909.
54. Klimov DK, Thirumalai D. Mechanisms and kinetics of β-hairpin formation. *Proc. Natl Acad. Sci. USA* 2000; **97**: 2544–2549.
55. Eaton WA, Muñoz V, Hagen SJ, Jas GS, Lapidus LJ, Henry ER, Hofrichter J. Fast kinetics and mechanisms in protein folding. *Annu. Rev. Biophys. Biomol. Struct.* 2000; **29**: 327–359.
56. Daura X, Glättli A, Gee P, Peter C, van Gunsteren WF. Unfolded state of peptides. *Adv. Prot. Chem.* 2002; **62**: 341–360.